

# Hard and Soft X-ray Absorption Spectroscopic Investigation of Aqueous Fe(III)–Hydroxamate Siderophore Complexes

David C. Edwards<sup>\*,†</sup> and Satish C. B. Myneni<sup>‡,§</sup>

Department of Chemistry, Frick Laboratory, Princeton University, Princeton, New Jersey 08544, Department of Geosciences, Princeton University, Guyot Hall, Princeton, New Jersey 08544, and Earth Sciences Division, Lawrence Berkeley National Laboratory, Berkeley, California 94720

Received: June 21, 2005; In Final Form: September 7, 2005

Microorganisms release organic macromolecules, such as siderophores, to obtain Fe(III) from natural systems. While the relative stabilities of Fe(III)–siderophore complexes are well-studied, the structural environments of Fe(III) and ligands in the complex are not well-understood. Using the X-ray absorption spectroscopy (XAS) at the Fe- and N-K absorption edges, we characterized the nature of Fe(III) interactions with a hydroxamate siderophore, desferrioxamine B (desB), and its small structural analogue, acetohydroxamic acid (aHa), as a function of pH (1.4–11.4). These experimental studies are complemented with DFT calculations. The Fe-XAS studies suggest that Fe(aHa)<sub>3</sub> is the dominant species in aqueous solutions in the pH range of 2.8–10.1, consistent with thermochemical information. However, the N-XAS and resonance Raman studies show that the chemical state of the ligand in the Fe(aHa)<sub>3</sub> complex changes significantly with pH, and these variations are correlated with further deprotonation of the Fe(aHa)<sub>3</sub> complex. The N-XAS studies also indicate that the overlap of Fe 3d orbitals with the molecular orbitals of the hydroxamate group is significant. The Fe- and N-XAS studies of Fe(III)–desB complexes indicated that Fe(desB)<sup>+</sup> is the dominant species between pH values of 1.4 and 11.4, consistent with predicted stability constants. This information is useful in understanding the role of iron in bacterial transport, siderosis treatment, and actinide sequestration at contaminated sites. This is the first N-XAS study of aqueous metal ligand complexes, which demonstrates the applications of soft-XAS in studying the electronic structure of metal complexes of organic macromolecules in aqueous solutions.

## Introduction

The hydroxamate functional group (CONROH, R = H, (CH<sub>2</sub>)<sub>n</sub>) is an important ferric iron chelating moiety in microbial siderophores: organic macromolecules secreted by bacteria in iron-limiting environments.<sup>1–3</sup> The hydroxamate moieties in siderophores effectively compete with other organic molecules (carboxylic acids, humic substances) for iron because of their high binding constants (5–10 orders of magnitude higher than others).<sup>4,5</sup> The trihydroxamate siderophore, desferrioxamine B (desB), is one of the most common siderophores in soil ( $\mu$ M concentration) and aqueous (nM concentration) systems and has an Fe(III) binding constant ( $\log \beta$ ) of 32.6 in aqueous solutions (Figure 1).<sup>6–8</sup> It forms a hexadentate complex with Fe(III), and the Fe(desB)<sup>+</sup> species dominates in the pH range of 1–12 (Figure 2).<sup>7</sup> Although the importance of Fe–siderophore complexes in the cellular transport of iron, treatment of siderosis, and sequestration of actinides from radioactive waste repositories has been established, the coordination environment and the structures of metal–siderophore complexes in aqueous solutions are not well-understood.<sup>9–11</sup> A previous structural analysis of these complexes was limited to the isolated crystalline compounds in the dry state.<sup>12</sup> The identification of the structure and speciation of Fe(III)–siderophore complexes as a function of pH in aqueous solutions is necessary in understanding the role of siderophores in the aforesaid processes.

\* Corresponding author. E-mail: dedwards@wesleyancollege.edu.

<sup>†</sup> Department of Chemistry, Princeton University.

<sup>‡</sup> Department of Geosciences, Princeton University.

<sup>§</sup> Lawrence Berkeley National Laboratory.

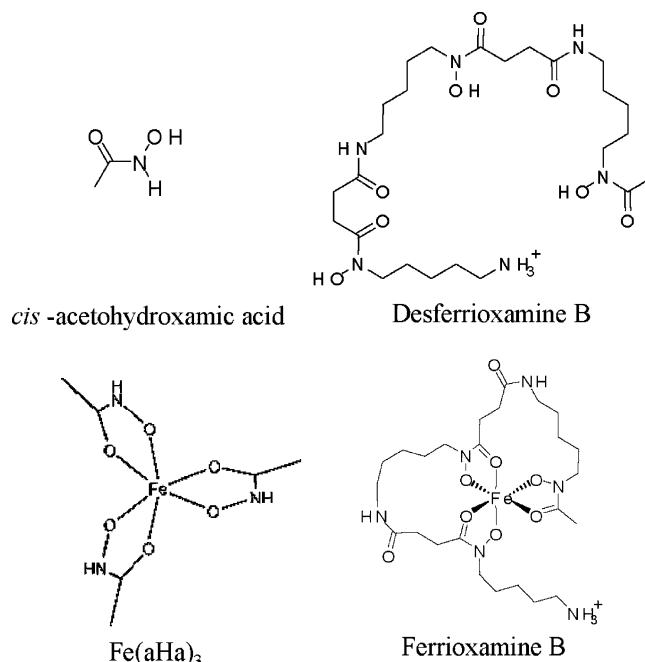


**Figure 1.** Structural representations of acetohydroxamic acid, desferrioxamine B, Fe(aHa)<sub>3</sub>, and Fe(desB)<sup>+</sup>.

Among different spectroscopic methods, vibrational spectroscopy (infrared, Raman, and resonance Raman) is widely used to explore the structures of ligands, and X-ray absorption spectroscopy (XAS) is used to study the metal coordination in

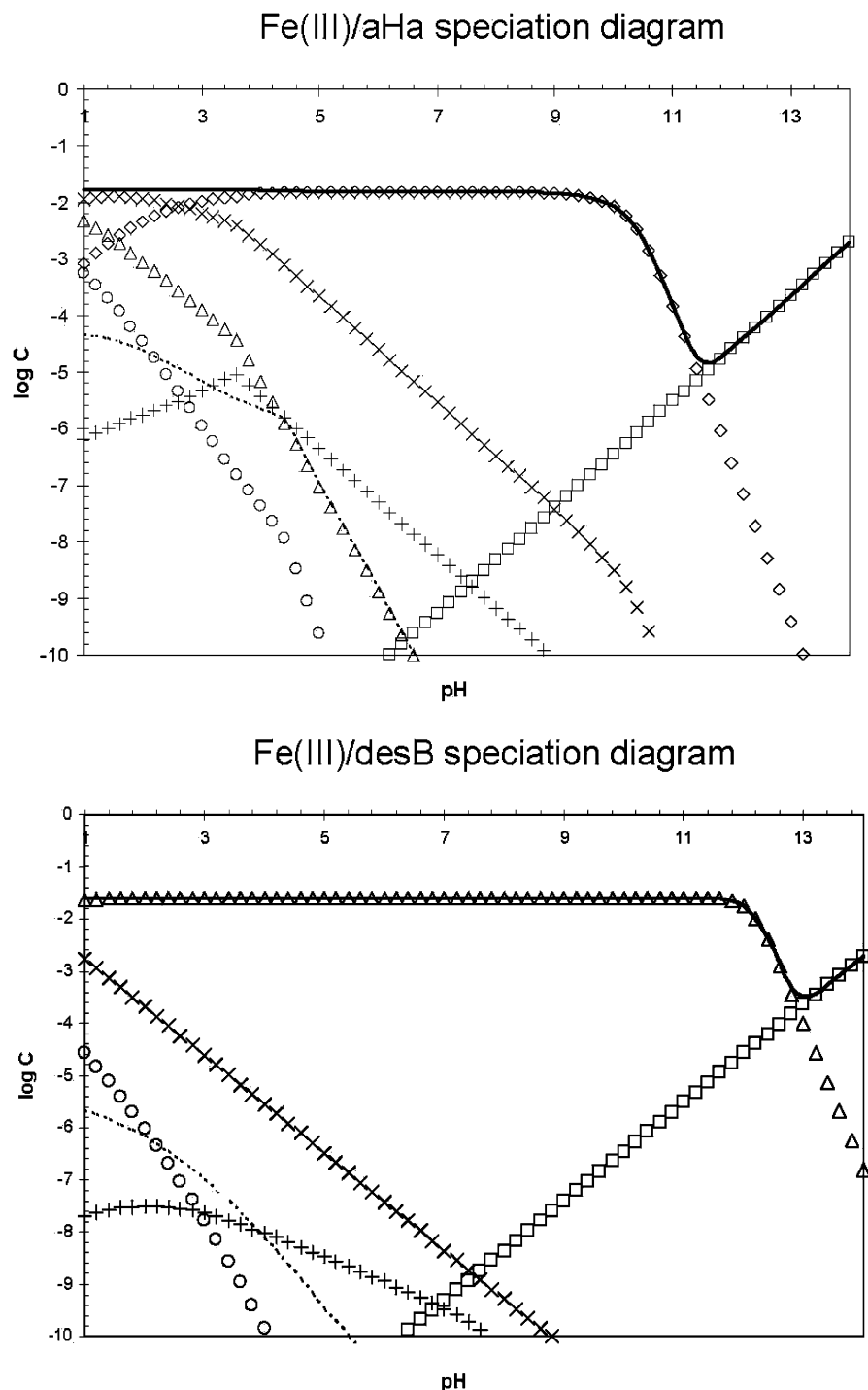


**Figure 2.** Thermodynamic speciation diagrams for Fe(III) aHa and desB in equilibrium with ferrihydrite. Fe(III)–aHa diagram calculated for  $[\text{Fe(III)}] = 17 \text{ mM}$  and  $[\text{aHa}] = 50 \text{ mM}$ . Total iron (—),  $\text{Fe(aHa)}_2^{2+}$  ( $\Delta$ ),  $\text{Fe(aHa)}_2^{+}$  ( $\times$ ),  $\text{Fe(aHa)}_3$  ( $\diamond$ ),  $\text{Fe}^{3+}$  ( $\circ$ ),  $\text{Fe(OH)}_2^{+}$  ( $+$ ),  $\text{Fe(OH)}_2^{2+}$  (---), and  $\text{Fe(OH)}_4^{-}$  ( $\square$ ). Fe(III)–desB speciation diagram calculated for  $[\text{Fe(III)}] = 25 \text{ mM}$  and  $[\text{desB}] = 25 \text{ mM}$ . Total iron (—),  $\text{Fe(HdesB)}^{+2}$  ( $\times$ ),  $\text{Fe(desB)}^{+}$  ( $\Delta$ ),  $\text{Fe}^{3+}$  ( $\circ$ ),  $\text{Fe(OH)}_2^{+}$  ( $+$ ),  $\text{Fe(OH)}_2^{2+}$  (---), and  $\text{Fe(OH)}_4^{-}$  ( $\square$ ). Ferric hydroxide precipitates in alkaline solutions, and this corresponds to the dip in total iron in the system.

aqueous metal–organic complexes.<sup>8,13</sup> Our previous infrared and resonance Raman spectroscopic studies of Fe(III) desferrioxamine complexes in aqueous solutions showed that the vibrational modes of the reactive oxime group ( $\nu_{\text{C=O}}$ ,  $\nu_{\text{N-O}}$ ) in desB changes significantly upon Fe(III) complexation. These studies also indicated more electron delocalization in the hydroxamate (CONO) core of the Fe complex than in the uncomplexed form of desB.<sup>8</sup> A detailed understanding of electron delocalization in the reactive moieties of these biomacromolecules is important for predicting the nature of siderophore–metal interactions.

However, vibrational spectral interpretation of Fe–siderophore complexes is complicated by the presence of multiple functional groups in biomacromolecules with multiple absorbance bands. The element-specific soft-XAS (e.g., the C- and N-XAS) alleviates these problems and provides direct information on the electronic state of the ligand and its metal complex.<sup>14–16</sup> In this investigation we show how soft-XAS, specifically the near-edge X-ray absorption fine structure (NEXAFS) spectroscopy, at the nitrogen K-edge is used to study the functional group chemistry of organic macromolecules and their metal complexes

in aqueous solutions. The extended X-ray absorption fine structure (EXAFS) spectroscopy at the iron K-edge is also used to complement the structural information obtained from soft-XAS.<sup>17</sup>

The spectroscopic studies of Fe(III)–desB complexes are complemented with the spectroscopic studies of acetohydroxamic acid (aHa; Figure 1), a small siderophore analogue that contains the reactive hydroxamate functional group.<sup>8</sup> The complexation constant of aHa with Fe(III) is about 4 orders of magnitude smaller than the binding constant of Fe(III)–desB complex in aqueous solutions ( $\log \beta$  for aHa = 28.8).<sup>18</sup> The lower complexation ability of aHa when compared to desB is attributed to a lower electron delocalization in the hydroxamate binding pocket of aHa.<sup>5,8</sup> This study gives insight into the structures of Fe(III)–hydroxamate siderophore complexes and shows the applications of soft-XAS in studying metal–organic macromolecule complexes in aqueous solutions.

### Experimental Details

**Samples.** Desferrioxamine B, acetohydroxamic acid, iron(III) chloride ( $\text{FeCl}_3 \cdot 6\text{H}_2\text{O}$ ), hydrochloric acid (HCl), and sodium hydroxide (NaOH) were obtained from Sigma-Aldrich and used without purification. The Fe(III)–aHa solutions prepared for the XAS studies composed of 50 mM aHa and 17 mM  $\text{FeCl}_3 \cdot 6\text{H}_2\text{O}$  and for resonance Raman composed of 100 mM aHa and 33 mM  $\text{FeCl}_3 \cdot 6\text{H}_2\text{O}$ . The Fe(III)–desB solutions were prepared by mixing equal amounts of 25 mM desB and  $\text{FeCl}_3 \cdot 6\text{H}_2\text{O}$ . The sample pH was adjusted with 0.2 M HCl and 0.2 M NaOH, and the sample pH was measured using an Orion 525A pH meter and a probe. All samples were stored at 4 °C until used. Samples prepared at pH > 10 showed visible iron oxide precipitates. The supernatants of these samples were examined after the precipitates were removed by centrifugation. All solutions were prepared using high-purity 18 M $\Omega$  cm<sup>-1</sup> water (Milli-Q Plus, Millipore).

**Details of Spectroscopy Studies.** *N-NEXAFS Spectroscopy:* Nitrogen K-edge NEXAFS spectroscopy was performed on beamline 8.0 at the Advanced Light Source (LBNL, Berkeley, CA), using the soft X-ray end station for environmental research (SXEER). This chamber was optimized for soft-XAS studies of aqueous solutions under ambient conditions (1 atm).<sup>19</sup> The atmospheric pressure was maintained inside the sample chamber by placing a 0.16  $\mu\text{m}$  silicon nitride window between the sample chamber and upstream ultrahigh vacuum environment. The aqueous samples were placed in a polypropylene straw and were exposed directly to the X-ray beam through a small slit in the straw. The straw was placed at approximately 3 mm from the silicon nitride window and oriented at 45° with respect to the incident beam. The sample chamber was filled with research grade He (99.9995%) to improve X-ray transmission and to minimize contamination by the atmospheric N<sub>2</sub>. A low-energy grating (380 lines/mm) was used for all N-NEXAFS spectroscopic studies. The entrance and exit slits were set to 50  $\mu\text{m}$  for aHa and 25  $\mu\text{m}$  for desB to minimize beam-induced sample alterations. Sample decay was noticeable for Fe(III)–desB (not for Fe(III)–aHa) after one scan (i.e., after 5 min) with 50/50  $\mu\text{m}$  slits. When there was sample decay, the pre-edge intensities increased with additional features in the pre-edge region. To alleviate this problem for Fe(III)–desB, the entrance and exit slits were closed to 25  $\mu\text{m}$ .

Ten reproducible NEXAFS scans were collected and averaged for each sample. The samples were replenished after five scans (about 25 min). The absorption spectra were recorded by detecting sample fluorescence (F) using a gallium arsenide

photodiode (Hamamatsu Corporation). The N-NEXAFS spectra were collected with a 0.2 eV step size in the pre- and postedge regions and with a 0.05 eV step size close to the main absorption edge. The spectra were normalized to the incident photon flux,  $I_0$ , measured simultaneously in the vacuum part of the beamline. The sample spectrum ( $F/I_0$ ) was also normalized with a blank water spectrum to remove scattering contributions of water, and absorption in the EXAFS region of the sample spectrum was set to 1. All spectra were calibrated using one of the transitions of N<sub>2</sub> gas ( $1s \rightarrow \pi^*$  transition at 401.1 eV).<sup>20</sup> The experimental spectra were deconvoluted using the software PeakFit (Jandel Scientific, CA). The pre- and postedge transitions were fit with Gaussian functions, while the edge feature was modeled with an arctangent function during spectral deconvolution. In this study the intensity variations of pre-edge features were considered since they can be obtained accurately from spectral deconvolution procedures. The intensities of spectral features in the main edge region were difficult to estimate and to correlate to chemical changes in the molecule because of the uncertainty of arctangent energy.

The X-ray spectra of Fe(aHa)<sub>3</sub> were also computed using a DFT code, StoBe.<sup>21</sup> Energy optimized structures of Fe(aHa)<sub>3</sub><sup>8</sup> complex used for these calculations were generated using Gaussian 92 at the DFT B3LYP/6-31G\* level of theory.<sup>22</sup> The StoBe<sup>21</sup> calculations performed at the N-edge used the gradient corrected exchange functional by Becke<sup>23</sup> and correlation functional by Perdew.<sup>24</sup> A detailed description of the calculation is explained in a previous paper.<sup>19</sup> To calibrate the calculated spectra, the absolute energy scale was shifted using the  $\Delta\text{Kohn-Sham}$  ( $\Delta\text{KS}$ ) approach, which computes the energy difference between the ground state and a one-electron core hole excited state.<sup>25</sup> The value of the ionization potential was further improved by adding a relativistic correction of 0.3 eV at the nitrogen edge.<sup>25</sup> The nature of molecular orbitals involved with different electronic transitions were evaluated using the program Molden.<sup>26</sup>

*EXAFS Spectroscopy.* The EXAFS spectra of Fe(III)–aHa and –desB complexes were collected for the Fe K absorption edge on beamline 4-3 at the Stanford Synchrotron Radiation Laboratory using a Si (220) double-crystal monochromator. The incident beam was detuned by 50% above the Fe K-edge to remove higher order harmonics. The slits were set to 2 × 10 mm for the collection of the EXAFS spectra. Aqueous samples were placed in 5 mm thick acrylic holders and contained using X-ray clean Kapton tape. The sample holder was placed at 45° with respect to the incident beam, and the fluorescence spectra were collected with a 13-element Ge-detector. Each sample spectrum was an average of 10 scans and was calibrated with the iron foil (first inflection point at 7112 eV).<sup>14</sup>

The EXAFS spectral analysis was conducted with EXAFS-PAK.<sup>27</sup> The spectral background was subtracted using a first-order polynomial, while the postedge region was fit with a third-order spline. The resulting  $\chi(k)$  and their Fourier transforms were fit with calculated phase and amplitude functions for the single and multiple scattering paths of Fe–O and Fe–C/N generated using FEFF7.<sup>28</sup> An energy-minimized Fe(aHa)<sub>3</sub> complex model was used to generate the theoretically derived phase and amplitude functions. During the fitting of EXAFS data, the coordination number (CN), bond distance ( $R$ ), Debye–Waller factor ( $\sigma^2$ ), and the phase shift ( $\Delta E_0$ ) were used as adjustable fitting parameters. The amplitude reduction factor ( $S_0^2$ ) was set at 0.9 for all the fits.

*Resonance Raman Spectroscopy.* Raman and resonance Raman spectra were obtained using an excitation wavelength

of 407 nm (Spectra Physics krypton laser) and a 270° back-scattering sample geometry. The laser beam (power 20 mW) was focused with a cylindrical lens onto a thin-walled glass capillary tube containing samples, and the scattered light was collected and focused onto a single spectrograph (Chromex) equipped with a charge-coupled device (CCD; Princeton Instruments). All samples were scanned 20 times (each 30 s) and averaged. Raman bands of *N,N*-dimethylformamide at 1662, 1439.7, 1406.6, and 1092.4 cm<sup>-1</sup> were used to calibrate all samples. The Raman spectrum of water was used to subtract water contributions from the sample.

## Results and Discussion

In aqueous solutions, the solubility of Fe(III) is extremely low close to neutral pH and the Fe(III) concentration increases in acidic and alkaline solutions (Figure 2). The concentration of Fe(III) close to neutral pH is approximately 10<sup>-8</sup> and 10<sup>-15</sup> M in the presence of amorphous (ferrihydrite) and crystalline (goethite) Fe(III)-oxyhydroxides, respectively. However, Fe(III) solubility is significantly enhanced in the presence of siderophores because of their high affinity for Fe(III).<sup>29</sup>

The complexation constants of aHa indicate that Fe(III) reacts with aHa and forms Fe(aHa)<sub>*n*</sub> (*n* = number of ligands coordinated to Fe(III)), with “*n*” varying between 0 and 3 based on the solution pH. Each hydroxamate group forms a five-membered ring with Fe(III) (Figures 1 and 2). Thermodynamic speciation of Fe(III)-aHa solutions (concentration of Fe(III) = 17 mM and aHa = 50 mM) in equilibrium with solid ferrihydrite is shown in Figure 2a. The complexation constants indicate that Fe(aHa)<sub>3</sub> complex dominates in the pH range of 3–9.5, with Fe(aHa)<sub>2</sub><sup>+</sup> and Fe(aHa)<sub>2</sub><sup>+</sup> in acid solutions and solid ferrihydrite in alkaline solutions. This speciation diagram differs from a previous study, which used different initial aHa and Fe(III) concentrations ([aHa]/[Fe(III)] = 10) and did not consider a solid iron species.<sup>5</sup> Equilibrium speciation with amorphous Fe(III)-oxide is a better representation of the solution speciation because of its ubiquitous presence in the near neutral pH range. Desferrioxamine B forms a hexadentate complex with Fe(III) with the formation of 3 five-membered rings within the hydroxamate group (Figure 1). Speciation calculations conducted for the solution conditions examined in this study (concentration of desB and Fe(III) = 25 mM) indicate that the Fe(desB)<sup>+</sup> complex is dominant in the pH range of 1–12 (Figure 2).

The XAS studies of Fe(III)-aHa and Fe(III)-desB solutions were conducted at the Fe- and N-edges. The XAS studies at the Fe-edge focused on the EXAFS spectral features, which provided information on the structures of Fe-siderophore complexes and the changes in the coordination environment of Fe(III), whereas the N-NEXAFS provided clues on the structural changes of the ligand. During the preparation of the alkaline Fe(III)-aHa and -desB complexes, a significant concentration of Fe(III) precipitated out (probably as amorphous iron hydroxide or as ferrihydrite) of solution. However, these solutions exhibited brick red color after centrifugation and removal of the precipitate. This solution color is indicative of the presence of Fe(III)-ligand complexes in aqueous solutions when compared to the yellowish color of free aqueous Fe(III). These supernatant samples were used for XAS analysis of alkaline solutions. A summary of XAS studies indicated that the coordination environment around Fe(III) did not vary for both aHa and desB (from Fe-EXAFS), while the electronic state of the aHa changed significantly (from N-NEXAFS) as a function of pH.

**Fe-EXAFS Spectroscopy.** To identify the oxidation state and the coordination environment of Fe, the X-ray absorption spectra

of Fe(III)-aHa and Fe(III)-desB solutions were compared with the spectra of acidic Fe(III) solutions containing the [Fe(H<sub>2</sub>O)<sub>6</sub>]<sup>3+</sup> complex. Close examination of the absorption edges of these solutions indicate that the energies of white lines are similar for all these solutions, which indicates that a majority of Fe in aHa and desB complexes is in the ferric form. However, the EXAFS spectra of aqueous solutions of Fe(III) in the presence and absence of the organic ligands are dissimilar. The EXAFS spectra of Fe(III)-aHa and Fe(III)-desB show asymmetry in their oscillations when compared to that of aqueous solutions containing [Fe(H<sub>2</sub>O)<sub>6</sub>]<sup>3+</sup>, indicating that scattering from nearby atoms is different in these samples (Figures 3 and 4). However, the EXAFS spectra of Fe(III)-aHa and Fe(III)-desB solutions are similar in acidic and alkaline solutions.

The Fourier transforms of the EXAFS spectra of solutions containing [Fe(H<sub>2</sub>O)<sub>6</sub>]<sup>3+</sup> exhibit a strong peak at 1.5 Å (uncorrected for phase) without any other prominent features (Figure 3). The spectral fits of these EXAFS spectra with the theoretically derived phase and amplitude functions indicate that the Fe-O bond distance is 2.01 Å and the coordination number with O is estimated to be close to 6. In contrast, the Fourier transforms of Fe(III)-aHa solutions exhibit two distinct shells at 1.5 and 2.2 Å (not corrected for phase). The first shell fits of the Fe(III)-aHa complex and [Fe(H<sub>2</sub>O)<sub>6</sub>]<sup>3+</sup> complex are similar (Table 1). The small second shell feature is fit with scattering from approximately 6 lighter atoms, such as C, N, or O, at a distance of 2.84 Å. The Debye-Waller parameter is also small for both the first and second shell fits, which suggests that Fe(III) is nearly octahedral and the distances to second shell atoms do not vary significantly (Table 1). Based on the second shell fits, the complex is identified as Fe(aHa)<sub>3</sub>. In the case of Fe(III)-aHa solutions, the sample pH did not modify their Fe-EXAFS spectra, which indicates that the coordination environment of the Fe(III)-aHa complex does not change in the pH range of 2.8–10.1. Although accurate determination of coordination number for weak backscatters is poor with the EXAFS spectral analysis, the Fourier transform magnitude for the second shell did not change as the sample pH was changed. The predicted bond distances and the coordination number from the EXAFS spectral analysis are also similar to those measured for the crystalline Fe(aHa)<sub>3</sub> using X-ray diffraction.<sup>30</sup>

The EXAFS spectra and their Fourier transforms of Fe(III)-desB and Fe(III)-aHa complexes are similar (Figure 4a,b). The Fourier transforms Fe(III)-desB complexes showed three distinct shells at 1.5, 2.2, and 3.5 Å (uncorrected for phase). The coordination number and the bond distance estimates are ~6 O atoms at 2.01 Å for the first shell and ~6 C/N/O atoms at 2.84 Å for the second shell, respectively (Table 1). However, the  $\sigma^2$  for the second shell is smaller for the Fe(III)-desB complex when compared to that of the Fe(III)-aHa complex, which suggests that the Fe(III)-desB complex is more rigid with small variations in the second shell atom distances. Although the third shell could be fit with close to 13 C/N/O atoms at 4.06 Å, it is difficult to estimate the coordination number of light atoms this far from the absorber. It should also be noted that the  $\sigma^2$  for this shell is high. Fits with multiple scattering paths for this shell were also poor. The parameters derived from EXAFS spectral analysis are also consistent with the previously determined X-ray diffraction analysis of crystalline ferrioxamine B.<sup>11</sup> The EXAFS spectra of Fe(III)-desB solutions are also invariant with the sample pH (1.4–11.4), which suggests that Fe(III)-desB complex is stable in the examined pH range.

The Fe-EXAFS spectroscopy results are not entirely consistent with thermodynamic speciation discussed above (Figure



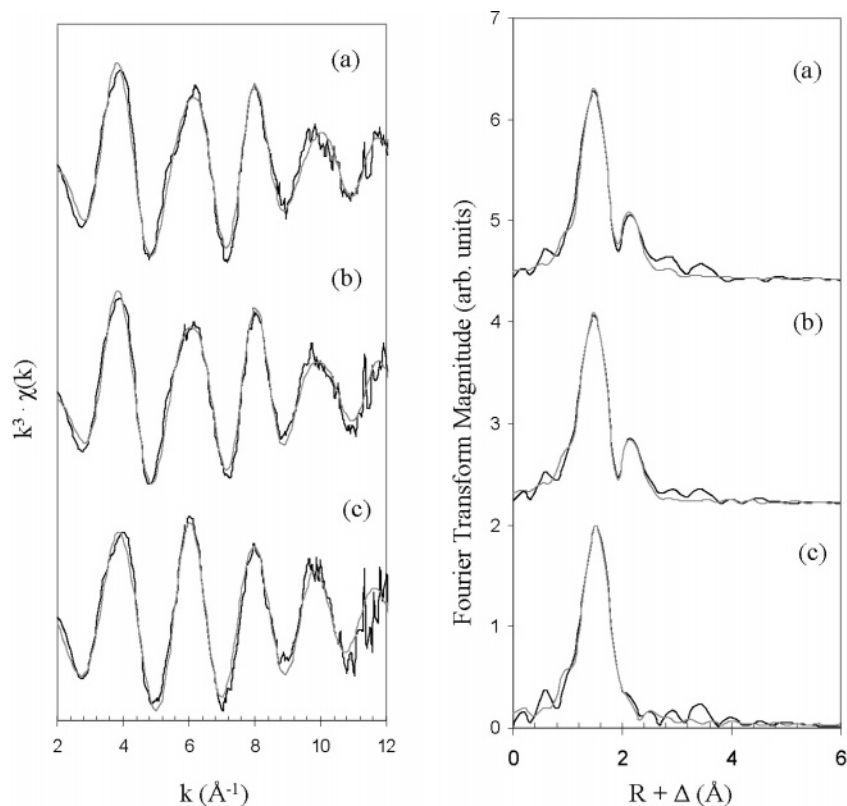


**Figure 3.** Fe-EXAFS ( $k^3$ -weighted) and their Fourier transforms of Fe(III)–aHa solutions at pH = 2.8 (a) and pH 10.1 (b). The EXAFS spectrum of 0.1 M FeCl<sub>3</sub> is shown in (c).

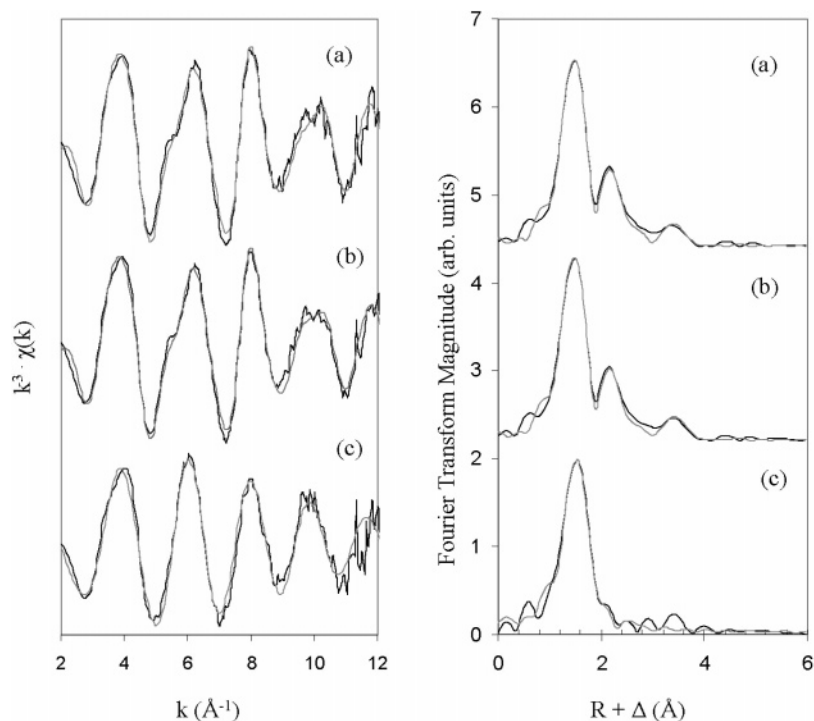


**Figure 4.** Fe-EXAFS ( $k^3$ -weighted) and their Fourier transforms of Fe(III)–desB solutions at pH = 1.4 (a) and pH 11.4 (b). The EXAFS spectrum of 0.1 M FeCl<sub>3</sub> is shown in (c).

2). Although it is difficult to distinguish Fe(aHa)<sub>3</sub> and Fe(aHa)<sub>2</sub><sup>+</sup> complexes in acid solutions using Fe-EXAFS alone, the spectral fits do not indicate any variations in the coordination environment of the second shell. In acid solution, multiple Fe<sup>3+</sup>–aHa complexes and uncomplexed Fe<sup>3+</sup> are expected from thermodynamic speciation and this should result in changes in the second shell parameters in the EXAFS spectral analysis

(especially for coordination number). This is not observed in our experimental EXAFS spectral analysis. In the case of desB, the total dissolved iron does not correlate with the Fe(III)–desB speciation diagram at high pH values. According to the diagram, all of the iron in the system is in the dissolved state until a pH of 12. However, we found visible solid iron precipitate in high pH Fe(III)–(desB) solutions. These results

**TABLE 1: Structural Parameters Derived from EXAFS Spectral Analysis<sup>a</sup>**

sample	Fe–O shell			Fe–C/N			Fe–C shell			$\Delta E_0$ (eV)
	CN	$R$ (Å)	$\sigma^2$ (Å)	CN	$R$ (Å)	$\sigma^2$ (Å)	CN	$R$ (Å)	$\sigma^2$ (Å)	
0.1 M FeCl <sub>3</sub>	6.6	2.04	0.007							–1.2
Fe(III)–aHa pH = 2.8	6.1	2.02	0.008	6	2.82	0.01				–5.2
Fe(III)–aHa pH = 10.1	6.1	2.01	0.008	5.4	2.85	0.008				–4.8
Fe(III)–desB pH = 1.4	6.3	2.01	0.007	5.4	2.84	0.004	12.6	15.5		–5.8
Fe(III)–desB pH = 11.4	6.9	2.01	0.006	6.2	2.84	0.004	4.06	4.06		–5.8
Fe(aHa) <sub>3</sub> <sup>b</sup>	6	2.01	0.0013	6	2.831	0.0014				
Fe(desB) <sup>+</sup> <sup>c</sup>	6	2.01	0.0009	6	2.84	0.0017				

<sup>a</sup> CN = coordination number ( $\pm 17\%$ ),  $R$  = interatomic distance ( $\pm 0.01$  Å),  $\sigma^2$  = Debye–Waller factor. <sup>b</sup> Data taken from X-ray crystal structure of Fe(aHa)<sub>3</sub>, Failes and Hambley, *Aust. J. Chem.* **2000**, 53, 879. <sup>c</sup> Data taken from X-ray crystal structure of Fe(desB)<sup>+</sup>, Dhungana et al. *J. Biol. Inorg. Chem.* **2001**, 6, 810.

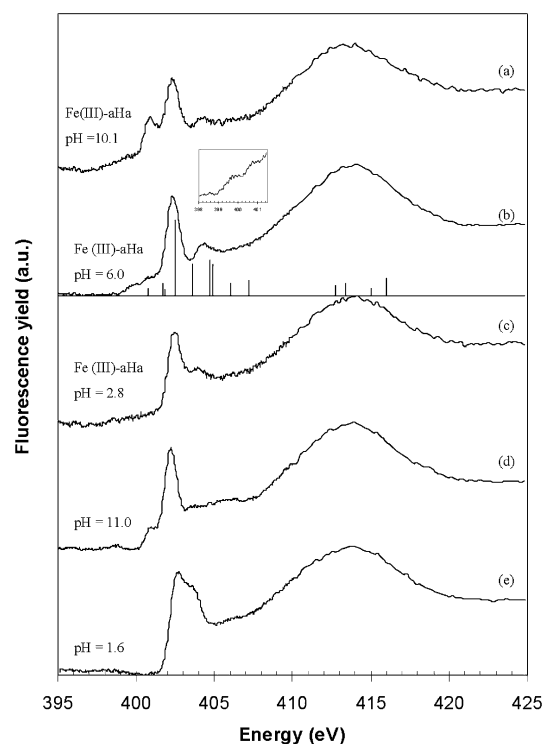


**Figure 5.** N-NEXAFS spectra of aHa and its Fe(III) complexes. The spectra “a”–“c” correspond to the Fe(III)–aHa solutions at pH 10.1, 6.0, and 2.8, respectively. The spectra “d” and “e” correspond to aHa at a pH of 11.0 and 1.6, respectively. Vertical solid lines for “b” are the normalized intensities for different electronic transitions calculated using Fe(aHa)<sub>3</sub> model. The inset highlights the pre-edge features in spectrum “b”.

indicate that the complexation constants may not accurately represent the stabilities of different complexes at low and high pH values.

**N-NEXAFS Spectroscopy.** The hydroxamate functional group is common for both aHa and desB, and its corresponding  $\pi^*_{(C=O)NO}$  transitions are expected to be similar in both molecules as a function of pH and Fe(III) complexation. Desferrioxamine B also exhibits additional features that correspond to the amide and amine, which are absent in aHa.

The N K-edge NEXAFS spectrum of aHa exhibits a distinct  $\pi^*_{(C=O)NO}$  transition at 402.5 ( $\pm 0.1$  eV) eV and a  $\sigma^*_{N-O}$  transition at 403.5 eV in acidic solutions (Figure 5, Table 2). Upon deprotonation of the oxime (N–OH) group, the peak corresponding to the  $1s \rightarrow \pi^*_{(C=O)NO}$  shifts to lower energy by 0.3 eV. This shift is caused by the increased electron delocal-

**TABLE 2: Experimental N-NEXAFS Spectral Transitions of aHa, desB, Fe(III)–aHa, and Fe(III)–desB<sup>a</sup>**

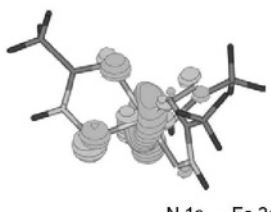
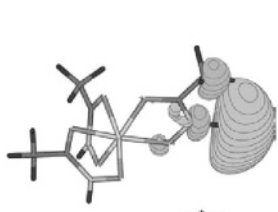
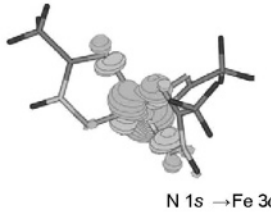
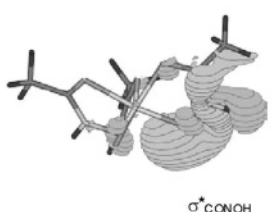
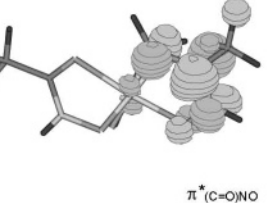
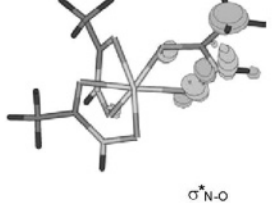
	aHa		Fe(III)–aHa		
	energy (eV)	intensity	energy (eV)	intensity	
pH = 1.6	402.5	1	pH = 2.8	402.4	1
	403.5	0.7		404	0.2
	413.4	1		411	0.3
pH = 8.6	401.1	0.1	pH = 6.0	399.8	0.7
	402.5	1.2		400.9	0.2
	403.6	0.6		402.3	1.3
pH = 11.0	413.5	1.2	pH = 10.1	403.4	0.3
	400.9	0.3		413.5	1
	402.2	1.5		399.5	0.1
	413.4	1.2	400.9	0.6	
			402.3	1.1	
			404.2	0.1	
			412.1	0.6	
		desB		Fe(III)–desB	
		energy (eV)	intensity	energy (eV)	intensity
pH = 4.9	401.2	0.4	pH = 1.4	401.3	0.3
	402.6	0.6		402.5	0.5
	403.3	0.2		413.1	1
pH = 8.2	401.2	0.4	pH = 4.3	401.3	0.3
	402.5	0.5		402.5	0.4
	403.2	0.1		413.9	1.3
pH = 10.3	401.2	0.3	pH = 11.4	401.3	0.3
	402.3	0.6		402.5	0.5
	406	0.3		414.5	1.1

<sup>a</sup> Peak locations were determined using the program PeakFit.

ization in the hydroxamate core (CONO) to accommodate excess negative charge from deprotonation. The  $\sigma^*_{N-O}$  transition at 403.5 eV disappears after deprotonation, although calculations indicate that it becomes weak and shifts to high energy ( $>404$  eV). All aHa sample spectra also exhibit a broad,  $\sigma^*_{N-C}$  transition at  $\sim 413$  eV, which is invariant with aHa protonation and Fe(III) complexation (Figure 5).

The N-NEXAFS spectra for the Fe(III)–aHa complex as a function of pH are shown in Figure 5 and the peak energies are given in Table 2. The calculated Fe(aHa)<sub>3</sub> transitions are shown in Figure 5b and Table 3. At low pH, the iron complex exhibits an intense transition at 402.4 eV, consistent with the  $\pi^*_{(C=O)NO}$  transition at 402.5 eV in the calculated model (Figure 5). At higher pH values, the  $\pi^*_{(C=O)NO}$  transition shifts to 402.3 eV (Figure 5a,b), which is similar to the deprotonated aHa (Figure 5d).<sup>19</sup> This decrease in energy as a function of pH may be ascribed to more electron delocalization in the hydroxamate group and an increase in complex strength. The transition around 404.0 eV is constant for all pH values and is attributed to a

**TABLE 3:** Calculated Transitions and Orbital Structures at the N K-Edge for Fe(aHa)<sub>3</sub>

energy (eV)	osl <sup>a</sup>	energy (eV)	osl <sup>a</sup>
400.8	0.00024	403.6	0.0046
			
N 1s → Fe 3d		σ* <sub>N-H</sub>	
401.7	0.00064	404.7	0.0039
			
N 1s → Fe 3d		σ* <sub>C=O/NOH</sub>	
402.5	0.011	404.9	0.0063
			
π* <sub>(C=O)NO</sub>		σ* <sub>N-O</sub>	

<sup>a</sup> osl = oscillator strength.

combination of  $\sigma^*_{N-H}$ ,  $\sigma^*_{N-O}$ , and  $\sigma^*_{(C=O)NOH}$  transitions (Figure 5b, Table 3).

The Fe(III)–aHa spectra also exhibit pre-edge transitions corresponding to the interactions of Fe 3d orbitals with the molecular orbitals of aHa (Figure 5a–c; Table 3). The pre-edge appears as a weak feature at ~400 eV in acid solutions, and as two discrete peaks at 399.8 and 400.9 eV in neutral and alkaline solutions. These transitions are assigned to the N 1s → Fe 3d orbitals, and the doublet at 399.8 and 400.9 eV corresponds to the transitions into  $d_{z^2}$  and  $d_{x^2-y^2}$  orbitals, respectively (Table 3). In highly alkaline solutions the peak intensity at 400.9 eV increases (Figure 5a), and the calculations indicate that this is due to a  $\pi^*_{(C=O)NO}$  transition from N-deprotonation of Fe(III)–aHa complex.<sup>19</sup> The major difference between this  $\pi^*_{(C=O)NO}$  transition and the one from O-deprotonation is that more charge is localized on the C–N bond in the N-anion than the O-anion.<sup>19</sup> The nonresolved features around 399 eV in the pre-edge region indicate that the complex is still intact in alkaline solutions, but may be in a different form than the Fe(III)–aHa complexes at lower pH values (Table 2). The presence of these complexes in alkaline solutions is also supported by the EXAFS spectral data.

The structure(s) of Fe(III)–aHa complex at high pH values, however, is not fully resolved. The  $\pi^*_{(C=O)NO}$  transition at 402.3 eV indicates the presence of the N-protonated Fe(aHa)<sub>3</sub> complex, while the transition at 400.9 eV assumes the presence of an N-deprotonated complex. Because the  $\pi^*_{(C=O)NO}$  transition is due to contributions from the whole CONO core, it is unlikely that both transitions are from the same aHa ligand. This implies that there is a mixed (both N protonated and deprotonated) iron complex or a mixture of exclusively N-protonated and N-deprotonated Fe(III)–aHa complexes.

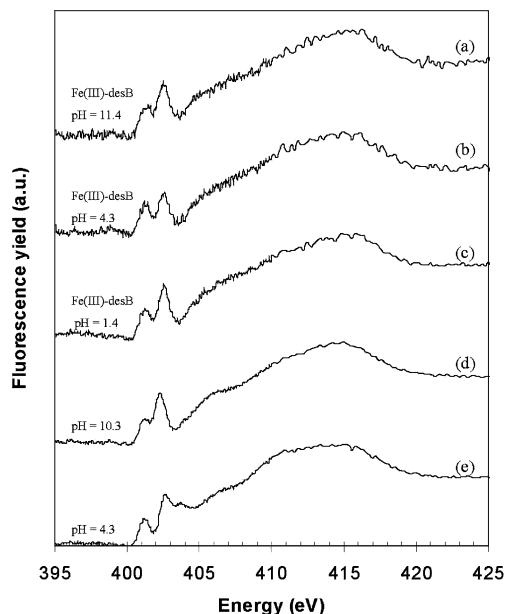


**Figure 6.** N-NEXAFS spectra of desB and its Fe(III) complexes. The spectra “a”–“c” correspond to the Fe(III)–desB solutions at pH 11.4, 4.3, and 1.4, respectively. The spectra “d” and “e” correspond to desB at a pH of 10.3 and 4.3, respectively.

When compared to aHa, desB has additional spectral features at 401.2 eV and ~406 eV that correspond to the amide  $\pi^*_{(C=O)NH}$  and amine  $\sigma^*_{N-H}$  transitions, respectively (Figure 6). These features do not change with pH because they are not involved in deprotonation. In addition, all the spectral features of aHa at 402.5 (1s →  $\pi^*_{(C=O)NO}$ ), 403.5 (1s →  $\sigma^*_{N-O}$ ), and 413 eV (1s →  $\sigma^*_{N-C}$ ) are also prominent in the N-NEXAFS spectrum of desB, and the first two transitions exhibit changes with variations in solution pH. The spectral features of Fe-complexed desB and anionic desB are also similar. The pre-edge doublet appeared in the case of Fe(III)–aHa solutions are absent or very weak in the case of Fe(III)–desB solutions. This may have been due to the presence of a strong amide  $\pi^*_{(C=O)NH}$  band at 401.2 eV, which overlaps with the low-energy pre-edge features.

**Resonance Raman Spectroscopy.** The resonance Raman spectra for the Fe(III)–aHa complexes in the pH range of 8.5–13 are shown in Figure 7. The prominent peaks of the Fe(III)–aHa complex at near neutral pH are the resonance-enhanced amide I band (a combination of  $\nu_{C=O}$  stretching and  $\nu_{C-N}$  stretching frequencies) at 1612  $\text{cm}^{-1}$  and the  $\nu_{N-O}$  stretching frequency at 997  $\text{cm}^{-1}$ . There is also a weak feature from the amide II band (a combination of  $\nu_{C-N}$  stretching and  $\delta_{N-H}$  bending modes) at 1540  $\text{cm}^{-1}$ . As the sample pH increases, the intensities of the amide I and amide II bands decrease and a new peak appears at 1570  $\text{cm}^{-1}$ . Because these are resonance Raman spectra, the new feature is likely due to a new Fe(III)–aHa complex forming in solution at high pH values. One possibility is an Fe(III)–hydroxamido complex (deprotonated N atom in the hydroxamate core), which is consistent with the decrease in the amide I band and the decrease in intensity of the  $\nu_{N-O}$  stretching frequency with increasing pH (calculated N-deprotonated models of the hydroxamate indicate the  $\nu_{N-O}$  frequency decreases and shifts to lower energies).<sup>8</sup> Infrared spectra in the same pH range (data not shown) do not have the appearance of a new peak in the amide I region; rather, the IR spectrum resembles the aHa anion in aqueous solutions.<sup>8</sup> This implies that the new complex has a symmetry-forbidden transition in IR or is below the detection limits of the IR spectrometer. At a pH of 12.3, the amide I band at 1570  $\text{cm}^{-1}$  is dominant and the  $\nu_{N-O}$  stretching frequency is almost absent,

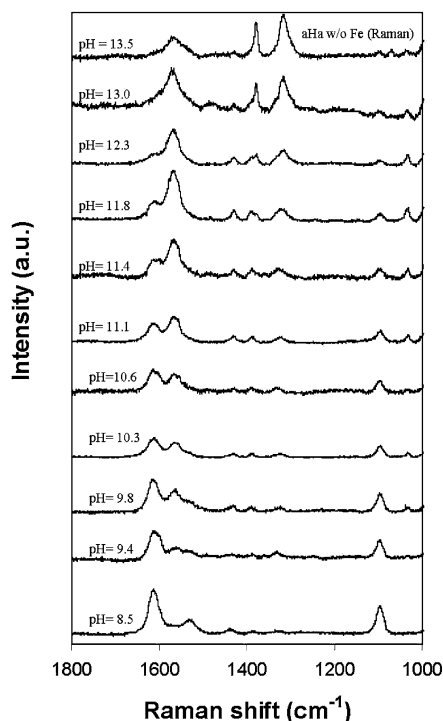


**Figure 7.** Resonance Raman spectra of the Fe(III)–aHa in alkaline solutions. The top spectrum is a Raman spectrum of aqueous aHa without iron.

indicating that the complex dissociated in these alkaline solutions. At a pH of 13, aHa is not complexed with Fe(III), which is evident from an increase in the intensities of the  $\delta_{\text{CH}_3}$  bending modes in the 1300–1400  $\text{cm}^{-1}$  range that are similar to the aqueous solution spectrum of the aHa anion (top spectrum in Figure 7). The resonance Raman spectra verify the presence of a new Fe(III)–aHa complex, but the identity of the complex remains unknown.

### Speciation Summary

With use of a combination of metal and ligand XAS and resonance Raman spectroscopy, the structures of Fe(III)–aHa and Fe(III)–desB have been characterized as a function of pH. These studies indicate that Fe(III) forms stable complexes with aHa and desB in the pH range of  $\sim 1.5$ –11.5 and further suggest that the Fe(aHa)<sub>3</sub> complex is stable beyond the pH ranges predicted by the current thermodynamic constants. These studies also suggest that the coordination environment of the Fe center does not change appreciably in the Fe(aHa)<sub>3</sub> complexes; however, the ligand deprotonates further in alkaline solutions. In contrast, the coordination environment of the metal center and ligand in Fe(III)–desB complexes do not change in the entire pH range examined. The molecular information presented here is also useful for understanding cellular recognition of Fe–siderophore complexes and actinide sequestration.<sup>9,11</sup> A recent study proposed that one possible mechanism is the dissociation of the Fe(desB)<sup>+</sup> complex in a low pH (around 2.4) section inside the cell.<sup>9</sup> Our finding of a stable Fe(desB)<sup>+</sup> complex at pH values below 2.0 suggests that the cellular environment inside this section of the cell must be more acidic to promote dissociation of ferrioxamine B. Desferrioxamine B also has a propensity to bind actinides that have ionic radii similar to iron.<sup>11</sup>

These studies document how soft- and hard-XAS can be used in exploring the coordination environments of metal center and the functional groups in organic macromolecule complexes. This is the first study that evaluates the aqueous solutions of metal–

ligand aqueous complexes using soft-XAS in native sample conditions. This important development can lead to studies that evaluate other natural metal–organic complexes under pristine conditions with XAS. Theoretical calculations can also assist the experimental measurements in the accurate description of the electronic states of the metal–ligand complexes.

**Acknowledgment.** The authors would like to thank the EMSP and the BES (Chemical and Geosciences) programs of the DOE for funding this study, Dr. Thomas Spiro for helping with the Raman studies, and Drs. Juro Majzlan, Ashish Deshmukh, and Dan Blanchard for providing useful comments on the manuscript. D.C.E. is also supported by the Advanced Light Source Doctoral Fellowship and the Princeton Environmental Institute – Science, Technology and Environmental Policy Fellowship. All of the synchrotron studies were conducted at the SSRL and at the ALS, and these facilities are supported by the DOE.

### References and Notes

- (1) Carrano, C. J.; Raymond, K. N. *J. Bacteriol.* **1978**, *136*, 69.
- (2) Konetschny-Rapp, S.; Jung, G.; Raymond, K. N.; Meiwes, J.; Zahner, H. *J. Am. Chem. Soc.* **1992**, *114*, 2224.
- (3) Martinez, J. S.; Haygood, M. G.; Butler, A. *Limnol. Oceanogr.* **2001**, *46*, 420.
- (4) Morel, F. M. M.; Hering, J. G. *Principles and Applications of Aquatic Chemistry*; John Wiley & Sons: New York, 1993.
- (5) Holmen B. A.; Tejedor-Tejedor M. I.; Casey W. M. *Langmuir* **1997**, *13*, 2197.
- (6) Powell, P. E.; Cline, G. R.; Reid, C. P. P.; Szanislo, P. J. *Nature* **1980**, *287*, 833.
- (7) Schwarzenbach G.; Schwarzenbach K. *Helv. Chim. Acta* **1963**, *46*, 1390.
- (8) Edwards, D. C.; Nielsen, S. B.; Jarzecki, A. A.; Spiro, T. G.; Myneni, S. C. B. *Geochim. Cosmochim. Acta* **2005**, *69*, 3237.
- (9) Wirgau, J. I.; Crumbliss, A. L. *Inorg. Chem.* **2003**, *42*, 5762.
- (10) Birus, M.; Zdravko, B.; Kujundzic, N.; Pribanic, M. *Inorg. Chim. Acta* **1983**, *78*, 87.
- (11) Brainard, J. R.; Strietelmeier, B. A.; Smith, P. H.; Langston-Unkefer, P. J.; Barr, M. E.; Ryan, R. R. *Radiochim. Acta* **1992**, *58/59*, 357.
- (12) Dhungana, S.; White, P. S.; Crumbliss, A. L. *J. Biol. Inorg. Chem.* **2001**, *6*, 810.
- (13) Strathmann, T. J.; Myneni, S. C. B. *Geochim. Cosmochim. Acta* **2004**, *68*, 3441.
- (14) Stohr, J. *NEXAFS Spectroscopy*; Springer-Verlag: New York, 1992.
- (15) Gordon, M. L.; Cooper, G.; Morin, C.; Araki, T.; Turci, C. C.; Kaznatcheev, K.; Hitchcock, A. P. *J. Phys. Chem. A* **2003**, *107*, 6144.
- (16) Myneni S. C. B. *Rev. Mineral. Geochem.* **2002**, *49*, 485.
- (17) O'Day, P. O.; Rehr, J. J.; Zabinsky, S. I.; Brown, G. E. *J. Am. Chem. Soc.* **1994**, *116*, 2938.
- (18) Farkas, E.; Kozma, E.; Petho, M.; Herlihy, K. M.; Micera, G. *Polyhedron* **1998**, *17*, 3331.
- (19) Edwards, D. C.; Myneni, S. C. B. To be submitted to *J. Phys. Chem. A*.
- (20) Chen, C. T.; Ma, Y.; Sette, F. *Phys. Rev. A* **1989**, *40*, 6737.
- (21) Herrmann, K.; Pettersson, L. G. M.; Casida, M. E.; Daul, C.; Goursot, A.; Koester, A.; Proynov, E.; St-Amant, A.; Salahub, D. R. Contributing authors: Carravetta, V.; Duarte, H.; Godbout, N.; Guan, J.; Jamorski, C.; Lebeouf, M.; Malkin, V.; Malkina, O.; Nyberg, M.; Pedocchi, L.; Sim, F.; Triguero, L.; Vela, A. *StoBe-deMon version 1.0*; deMon Software, 2002.
- (22) Frisch, M. J.; Trucks, G. W.; Head-Gordon, M.; Gill, P. M. W.; Wong, M. W.; Foresman, J. B.; Johnson, B. C.; Schlegel, H. B.; Robb, M. A.; Replogle, E. S.; Gomperts, R.; Andres, J. L.; Raghavachari, K.; Binkley, J. S.; Gonzalez, C.; Martin, R. L.; Fox, D. J.; Defrees, D. J.; Baker, J.; Stewart, J. J. P.; Pople, J. A. *Gaussian 92, Revision C*; Gaussian Inc.: Pittsburgh, PA, 1992.
- (23) Becke, A. D. *Phys. Rev. A* **1988**, *38*, 3098.
- (24) Perdew, J. P. *Phys. Rev. B* **1986**, *34*, 7406.
- (25) Triguero, L.; Plashkevych, O.; Pettersson, L. G. M.; Agren, H. *J. Electron Spectrosc.* **1999**, *104*, 195.
- (26) G.Schaftenaar; Noordik, J. H. *J. Comput.-Aided Mol. Design* **2000**, *14*, 123.
- (27) George, G. N.; Pickering, I. J. *EXAFSPAK*; Stanford Synchrotron Radiation Laboratory: Menlo Park, CA, 1995.
- (28) Ankudinov, A. L.; Ravel, B.; Rehr, J. J.; Conradson, S. D. *Phys. Rev. B* **1998**, *58*, 7565.
- (29) Holmen, B. A.; Casey, W. H. *Geochim. Cosmochim. Acta* **1996**, *60*, 4403.
- (30) Failes, T. W.; Hambley, T. W. *Aust. J. Chem.* **2000**, *53*, 879.